ELSEVIER

Spectrochimica Acta Part B 60 (2005) 1392 – 1401

SPECTROCHIMICA ACTA PART B

www.elsevier.com/locate/sab

Effect of laser pulse energies in laser induced breakdown spectroscopy in double-pulse configuration

P.A. Benedetti, G. Cristoforetti *, S. Legnaioli, V. Palleschi, L. Pardini, A. Salvetti, E. Tognoni

Applied Laser Spectroscopy Laboratory, Institute for Chemical-Physical Processes, Research Area of National Research Council, Via G. Moruzzi, 1-56124 Pisa, Italy

Received 20 April 2005; accepted 15 August 2005
Available online 10 October 2005

Abstract

In this paper, the effect of laser pulse energy on double-pulse laser induced breakdown spectroscopy signal is studied. In particular, the energy of the first pulse has been changed, while the second pulse energy is held fixed. A systematic study of the laser induced breakdown spectroscopy signal dependence on the interpulse delay is performed, and the results are compared with the ones obtained with a single laser pulse of energy corresponding to the sum of the two pulses. At the same time, the crater formed at the target surface is studied by video-confocal microscopy, and the variation in crater dimensions is correlated to the enhancement of the laser induced breakdown spectroscopy signal. The results obtained are consistent with the interpretation of the double-pulse laser induced breakdown spectroscopy signal enhancement in terms of the changes in ambient gas pressure produced by the shock wave induced by the first laser pulse.

Keywords: LIBS; Laser; Spectroscopy; Double pulse; Confocal microscopy

1. Introduction

The laser induced breakdown spectroscopy (LIBS) performed in double-pulse (DP) configuration is a promising development of the traditional well-known LIBS, which makes use of a single laser pulse (SP) for the ablation of the sample. In the DP configuration a pair of pulses, delayed the one with respect to the other by a temporal gap of the order of 1–10 μs, is used for the ablation of material from the target surface and consequent formation of a plasma plume; the analysis of the plasma emission, acquired in a suitable temporal window, allows qualitative and quantitative information on the elemental composition of the sample.

The DP configuration maintains the benefits of the LIBS technique, such as the fastness, the absence of chemical pretreatment and the ability of in situ applications; however, it has been demonstrated that DP LIBS improves the limits of detection of the different chemical elements by one to two orders of magnitude, by increasing the discrete optical emission of the plasma plume.

Several DP configurations have been studied, differing on the geometrical configuration, the wavelength and the temporal order of the two laser beams. Mainly, the so-called parallel or collinear configuration is often used, where both the beams are directed perpendicularly to the target surface [1–5], but also the orthogonal configuration has been tested, where the first pulse (pre-pulse scheme) [6–10] or the second one (re-heating scheme) [11,12] is directed parallel to the target surface and focused in the ambient gas in front of it, while the other is perpendicular and ablates the target.

In spite of the numerous works dedicated to the DP LIBS configuration, the reason (or the concurrent reasons) of the signal improvement is still not completely clear.

In our previous works, all devoted to the study of DP LIBS in parallel configuration, we have presented a phenomenological model of the different ablation characteristics of the DP LIBS, using a time- and space-resolved emission analysis of the plume [13] and a study of the emission obtained at different ambient gas pressures and different interpulse delays with spectroscopic [14] and imaging techniques [15].

The present work is aimed to the study of the effect of the pulse energy on the LIBS signal enhancement in collinear configuration, to add another element to the comprehension of

* Corresponding author. Tel.: +39 50 3152222; fax: +39 50 3152230.
E-mail address: gabriele@ipcf.cnr.it (G. Cristoforetti).

0584-8547/$ - see front matter © 2005 Elsevier B.V. All rights reserved.
doi:10.1016/j.sab.2005.08.007

the physical processes involved in DP LIBS. In particular, since we hypothesized in the previous works that the benefits of double-pulse configuration are due to the effect of the first pulse, which "prepares" the ambient conditions where the second pulse can produce an optimal ablation, we focused our study on the effect of the first pulse energy on LIBS signal. In order to account for the different signal enhancements obtained with the different laser energies, we studied the thermodynamical parameters of the plasma and the mass ablated from the target.

The few previous works on this subject [12,16] were carried out in different experimental setups: Ray et al. [16] studied the effect of the energy of the first laser pulse in a DP LIBS experiment on a liquid jet while Gautier et al. [12] reported a study on both laser pulse energies but in the orthogonal DP configuration (both in the re-heating and in the pre-pulse schemes).

2. Experimental setup

The experimental setup used in this work is sketched in Fig. 1. The measurements were performed using a new dual-pulse mobile LIBS instrument (MODI—MObile Dual-Pulse Instrument) produced by Marwan Technology s.r.l. (Italy) in collaboration with our laboratory. The instrument incorporates a dual-pulse laser, constituted by a double-rod resonator pumped by a single flashlamp, emitting two collinear laser pulses of about 10 ns duration (FWHM) with energy per pulse variable between 50 and 150 mJ at a maximum repetition rate of 10 Hz. The interpulse delay can be set from 0 (single pulse) to 60 μs. The laser pulse energies can be varied independently for the two beams.

The energies of the pulses were calibrated by means of a Scientech thermopile and then monitored during the experiment by sending a small fraction of the laser beams to a fast photodiode coupled to a digital oscilloscope.

An aluminum target (Al 99%, Mn 0.3%, Mg 0.6%), with the surface perpendicular to the laser beams, was mounted inside the MODI experimental chamber, on a motorized table for positioning at the optimal lens-to-sample distance. The sample surface was previously polished and cleaned to increase the reproducibility of measurements.

The two beams were focused on the target surface by means of a 100-mm focal length lens; the lens to sample distance was set to 5 mm less than the lens focal length (95 mm), in order to avoid the air breakdown in front of the target [17] and to improve the stability of the plasma [18].

The space-integrated LIBS signal was collected through an optical quartz fiber (diameter = 600 μm, N.A. = 0.22), placed at 45° with respect to the beam axis at a 3-cm distance from the target surface, and sent to the MODI Echelle spectrometer ($\lambda/\Delta\lambda = 7500$) coupled with an intensified CCD camera, which provided for each acquisition a full spectrum in the range 200–900 nm.

All the experimental operations, including sample movement, settings of the laser (energy of the beams, delay between the pulses, repetition rate) and setting of the spectral acquisition parameters (number of spectra averaged, acquisition delay, CCD measurement gate and gain), were controlled by the MODI personal computer.

The delay between the laser pulses was changed between 0, corresponding to single pulse, and 50 μs. A delay time of acquisition of 700 ns was chosen in order to allow the decay of continuum, due to Bremsstrahlung radiation and free-bound electronic recombination; an acquisition gate of 500 ns was also chosen, which guaranteed well-visible emission signals in all the different experimental conditions analyzed, but still allowing a meaningful calculation of the

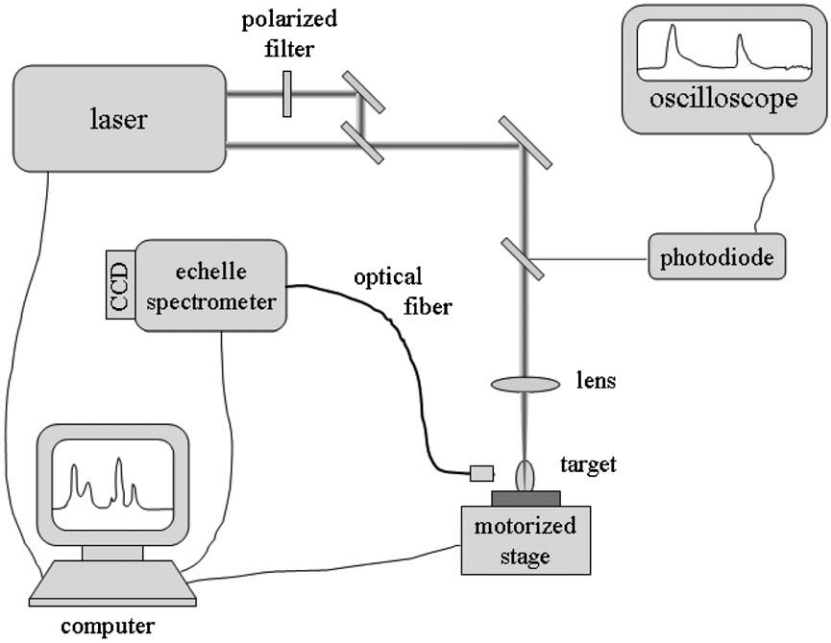

Fig. 1. Experimental setup used for spectroscopic analysis.

spatially integrated thermodynamical parameters of the plasma.

The energy of the first pulse was set to 13, 26, 39, 52, 65 and 78 mJ (corresponding to a fluence in the range 30–180 J cm^{-2} and irradiance in the range $3 \cdot 10^9$–$1.8 \cdot 10^{10}$ W cm^{-2}) while the energy of the second pulse was fixed to 78 mJ.

In order to reduce the spectral fluctuations, a series of 40 pairs of laser pulses was averaged for each measurement, at a repetition rate of 2 Hz.

In order to evaluate the crater volume obtained with single- and double-pulse LIBS, we examined the crater shapes using a ViCo (Biomedica Mangoni, Italy) video-confocal microscope (VCM) implemented on a Leica DM-RXA2 stand. As described elsewhere [19], in VCM an incandescent lamp may be used as a multi-point illumination source and a CCD camera as an image detector. The confocal imaging capability of VCM is guaranteed by an original processing method [20]. High resolution and flexibility joined with constructional simplification and economy are significant, especially when compared to single-point-scanning, laser-based confocal microscopes.

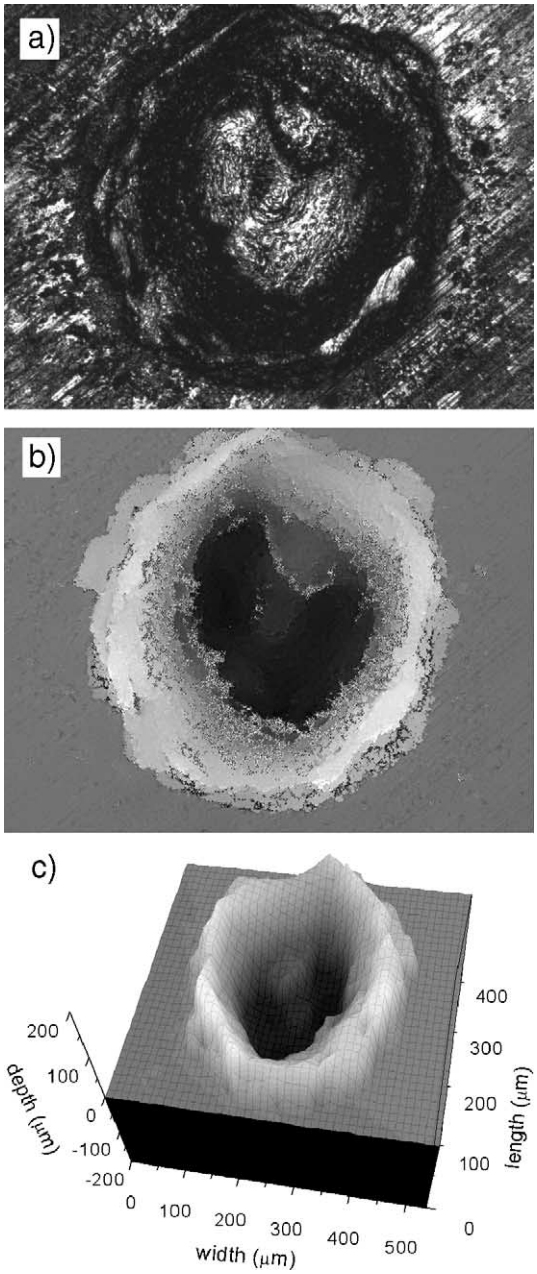

Fig. 2. Images of a typical crater analysed by video confocal microscopy: (a) extended focus image, (b) topographic image (each grey level correspond to a depth level) and (c) 3-D surface reconstruction.

For each crater, a stack of high-resolution optical sections has been collected at steps of 2 μm, along the focal axis. A dry objective (Leica 20×, 0.50 N.A.) has been employed in all measurements. Depending on actual crater depth, the overall range scanned along the focal axis was between 80 and 120 μm, with a total number of sections in the range of 40 or more.

In Fig. 2a, the extended focus image of a typical crater is presented, obtained by maximum projection of the reflectance signal taken from the set of focal sections corresponding to the field including the crater under measurement.

In Fig. 2b, the topographic image of the above crater is presented in which the depth information, corresponding to the maximum reflectance, has been calculated from the formerly described set of sections. Fig. 2c, finally, shows the plot of the surface of the same crater.

3. Results

3.1. Intensity measurements vs. delay between the pulses

For getting a better understanding of the effect of the first pulse in determining the formation and the evolution of the plasma plume produced in the DP LIBS, we performed the measurements fixing the second laser pulse energy E_2 at 78 mJ and changing the first laser pulse energy E_1 from 13 mJ up to 78 mJ, corresponding, respectively, to 1/6 and 6/6 of E_2. At the same time, the delay between the pulses was changed from 0 to 50 μs. The integrated intensities of Al I at 305.0 nm and Al II at 281.6 nm, as a function of the laser interpulse delay and at different energies of the first laser pulse, are reported in Fig. 3a and b, respectively. Both lines are not resonant, with a relatively high lower energy of the transition (29067 and 59852 cm^{-1}, respectively), so that self-absorption effects can be safely neglected in the intensity analysis.

Looking at the effect of the first pulse energy, a rapid growth of the line intensities between the lowest energy value E_1 and the other values is evident in both figures. The maximum signal obtained with $E_1 \geq 2/6E_2$ is 3 times higher for the neutral Al line and 4–6 times higher for the ionized Al line with respect to that obtained with $E_1 = 1/6E_2$. Moreover, whatever is the interpulse delay, the signal obtained is very similar for all the energies E_1 except the lowest one.

This suggests that the physical mechanism originating the signal improvement in the DP LIBS rapidly increases with E_1 for lower values and then saturates.

The LIBS signal enhancement of Al II at 281.6 nm in the DP configuration with respect to SP configuration at the same total energy is plotted in Fig. 4 (similar results are also obtained considering the Al I line at 305.0 nm). The highest improvement is obtained for $E_1 = 2/6E_2$ and decreases for

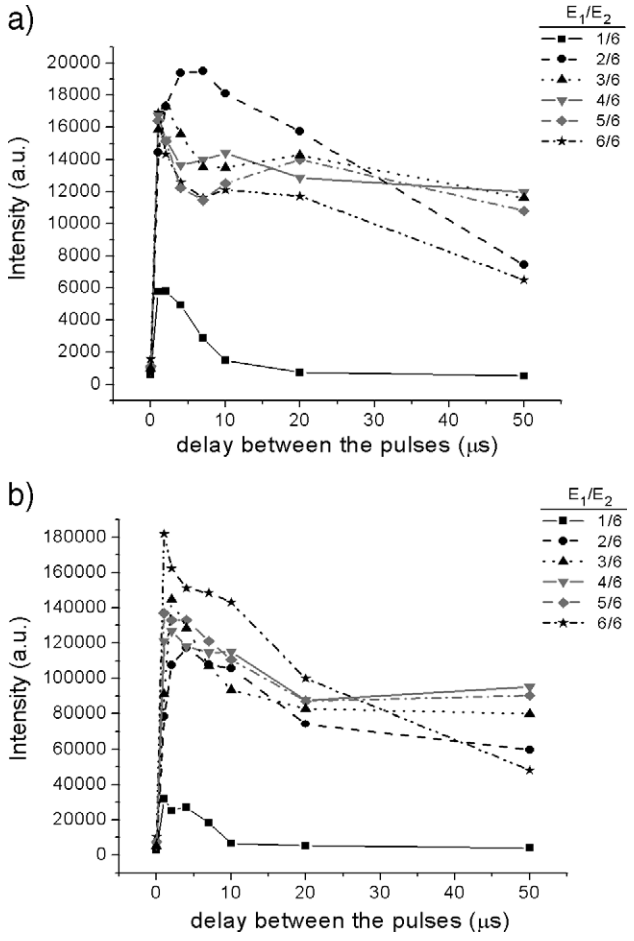

Fig. 3. Measured intensity of (a) Al I at 305.0 nm line and (b) Al II at 281.6 nm line as a function of the interpulse delay obtained for different values of the energy E_1 of the first laser pulse.

higher E_1 values. However, it should be noted that the reduction of the signal enhancement for $E_1 > 2/6E_2$ is due to the growth of the signal produced by the simultaneous pulses at laser energy E_1+E_2 and not to a real decrease of the intensity obtained in the DP case.

For all the energies, the highest signal enhancement is obtained for a delay between the two pulses in the range 1–4 μs, as previously found in many works [3,8,14]. For higher delays, the signal slowly decreases, except in the case of $E_1=13$ mJ, where the signal rapidly comes back to the value obtained with a single-pulse ablation.

In order to explain the trends of aluminum line intensities plotted in Fig. 3a and b, it is important to measure the evolution of temperature and electron densities in the plume and the ablated mass from the target, as described in the following.

3.2. Thermodynamical parameters vs. delay between the pulses

Both the spatially integrated temperature and electron density were calculated from the LIBS spectra acquired at different interpulse delays and different laser pulse energy.

The electron density was calculated by measuring the Stark broadening of H_α line, accounting for the quasi-static ion and impact-electron broadening effects, according to the formula [21]

$$n_e\ (\mathrm{cm}^{-3}) = 8.0210^{12}\left(\frac{\Delta\lambda_{1/2}}{\alpha_{1/2}}\right)^{3/2}$$

where $\Delta\lambda_{1/2}$ is the FWHM in Angstrom and $\alpha_{1/2}$ is a coefficient, weakly depending on electron density and temperature, tabulated by Griem [22]. Hydrogen emission is always present in the LIBS spectra taken in ambient air, because of the water vapor due to the natural humidity of the air. The use of hydrogen lines for electron density determination in laser plasmas has been already reported [23,24]; in the present work, we previously tested the reliability of the measurements by comparing the results with those found by measuring the Stark broadening of Mn II at 294.9 nm. We found that the values were in agreement within the experimental errors. However, the uncertainty affecting the electron density values obtained using the H_α line is lower (~10%) than the one corresponding to the values obtained using the Mn II line (~20–30%); this is due to the uncertainty in the determination of the line width.

The resulting values of the electron density do not show a clear behavior, considering the experimental error (10%) (see Fig. 5a), except in the case $E_1=E_2$ where a slight decrease in the DP case with respect to the simultaneous pulses is observed, as found elsewhere [2,13,14].

The plasma temperature has been also calculated, in the framework of the Local Thermal Equilibrium (LTE) approximation, using the Saha–Boltzmann plot method, as described in Ref. [25]. This method consists in a generalization of the Boltzmann plot which takes into account both neutral and ionized lines, through the use of the Saha equation and using the values of plasma electron density previously calculated. The lines used for temperature calculation are Al I at 265.2, 266.0, 305.0, 305.5, 305.7 nm and Al II at 281.6 nm. Using this technique, the maximum difference between the upper level energies of the transitions considered is ~106000 cm^{-1}, bringing to a considerable reduction of the fitting error with respect to the usual Boltzmann plot method. The experimental

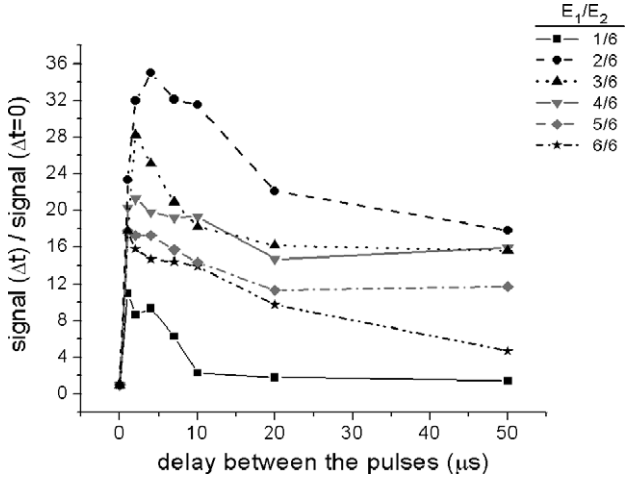

Fig. 4. Signal enhancement of Al II at 281.6 nm line in the DP configuration as a function of the interpulse delay obtained for different values of the energy E_1 of the first laser pulse.

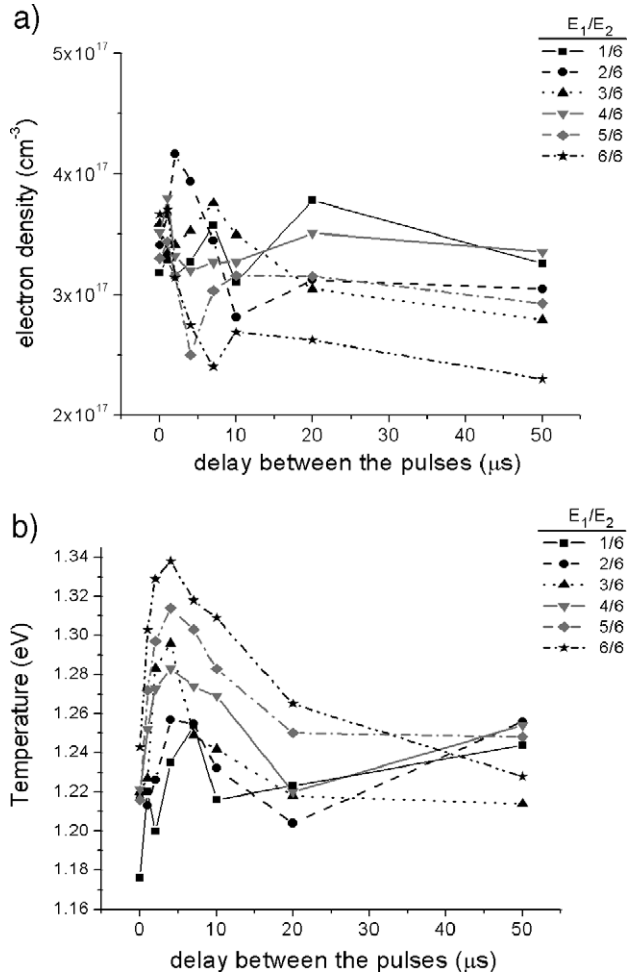

Fig. 5. Space-integrated thermodynamical parameters of the plasma as a function of the interpulse delay obtained for different values of the energy E_1 of the first laser pulse. (a) Electron density (cm^{-3}) (the experimental error is 10%). (b) Temperature (eV) (the experimental error is 3%).

errors on temperature calculation (neglecting the systematic error coming from the uncertainty of A_{ki} coefficients) are of the order of 3%, coming mainly from the uncertainties of the electron density and the fitting of the line profile.

The calculated plasma temperatures are plotted in Fig. 5b, as a function of the interpulse delay and for the different energies of the first laser pulse. For all the values of the energy of the first pulse, the maximum plasma temperature is reached for an interpulse delay in the range between 1 and 7 μs; a slow decrease then occurs with increasing the delay between the pulses. The increase of temperature in the DP experiments with respect to the SP case is consistent with the results of previous works [3,14] but is relatively small (of the order of 10%, around 0.05–0.1 eV) even at its maximum.

This observed small increase in temperature (together with the calculated value of electron density) cannot explain the LIBS signal enhancement evidenced in Fig. 4. In fact, the intensity enhancement R of a generic line in DP configuration with respect to single pulse can be written:

$$R = \frac{N_{DP}}{N_{SP}} \frac{n_{DP}}{n_{SP}} \frac{Z(T_{SP})}{Z(T_{DP})} \exp\left(-E_k \left(\frac{1}{k_B T_{DP}} - \frac{1}{k_B T_{SP}} \right) \right) \quad (1)$$

where N is the absolute total number of atoms of the chemical element considered, n is the fraction of these atoms corresponding to the emitting species (atomic or ionic), Z is the partition function, E_k is the upper energy level of the transition and k_B is the Boltzmann constant. In turn, the ratio n_{DP}/n_{SP} can be expressed in terms of the temperature and electron density values via the Saha equation.

Assuming at first that the total number N of emitting particles is the same in single- and double-pulse configuration, we calculated the expected signal enhancement for the neutral aluminum lines Al I at 265.3, 305.0, 308.2 nm and the ionized aluminum lines Al II at 281.6, 358.6, 466.3 nm for $E_1 = E_2 = 78$ mJ at an interpulse delay of 4 μs, based on the measurements of T and n_e. In that case, the small increment of temperature from 1.24 eV (simultaneous pulses) to 1.34 eV ($\Delta t = 4$ μs) results in a slightly higher population of higher energy levels and a slightly higher ionization, producing a negligible variation of the intensity of the neutral Al lines ($0.94 < R < 1.2$) and an increase of the ionized Al lines ($2.3 < R < 3$), as showed in Fig. 6a. The enhancement depends on the upper energy level of the transition and is well described by an exponential functions for both neutral and ionized species, according to Eq. (1).

This predicted behavior is similar to that observed in DP experiments performed in the re-heating orthogonal configuration, as found by Gautier et al. [11]. Our experiment confirms the increasing trend of the enhancement with the upper energy level; however, both neutral and ionized line show a substantial signal enhancement, as shown in Fig. 6b. Thus, although the increase of the temperature is certainly responsible of the trend of the signal improvement with the energy of the upper level, another mechanism is needed to model the actual experimental results.

In collinear DP configuration, the assumption that the ablated mass is the same than in single pulse is obviously unrealistic. In fact, by assuming an increase of the ablated mass in DP measurements equal to 7 (corresponding to $N_{DP}/N_{SP} = 7$ in Eq. (1)), the predictions of Eq. (1) well fit, within the experimental errors, the experimental data (see Fig. 6c).

It is thus clear that, to explain the enhancement of the LIBS signal in DP collinear configuration, it is necessary taking into account the higher ablated mass.

3.3. Crater measurements

In order to verify the correlation between the increase of the ablated mass and the LIBS signal enhancement in our experiment, we used the confocal microscopy setup above described for comparing the three-dimensional shape of the craters obtained in DP configuration, at an interpulse delay of 4 μs, with the ones obtained in single-pulse configuration, using a pulse energy $E_1 + E_2$. A profile of the craters obtained in the two configurations, at $E_1 = E_2 = 78$ mJ, is plotted in Fig. 7a and b. The crater produced in DP configuration is much deeper than that produced by a single laser pulse, as expected. Fig. 8a and b show the measured volume under the surface obtained in single-pulse configuration, as a function of the energy $E_1 + E_2$ of the pulse, and in DP configuration as a

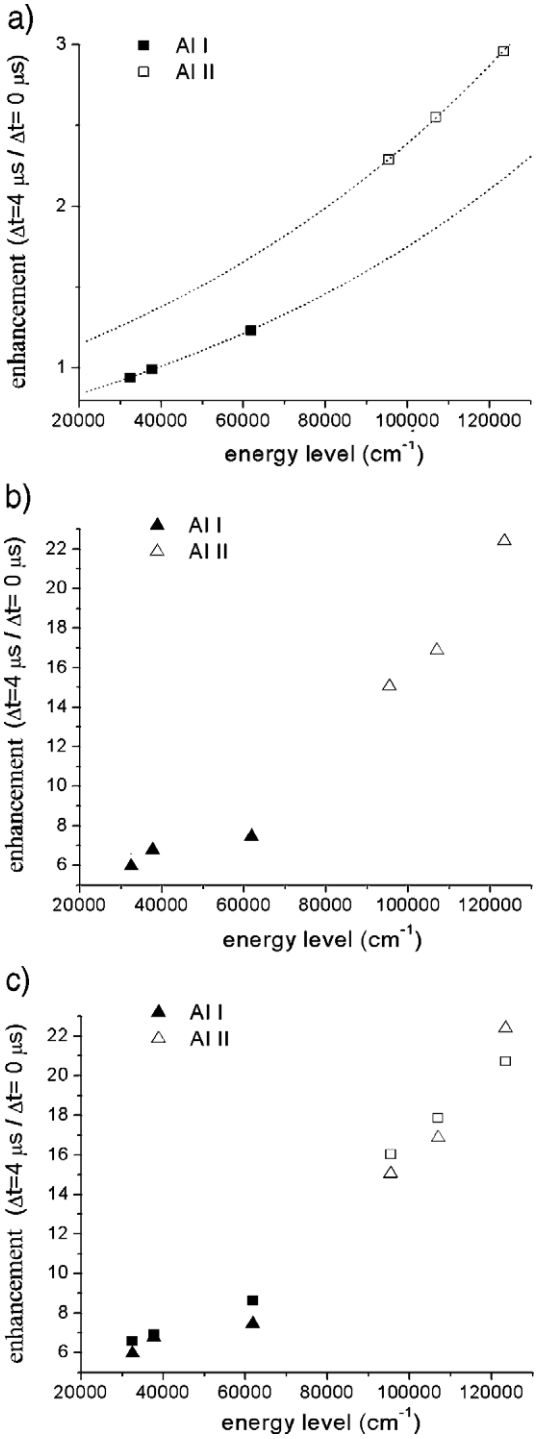

Fig. 6. (a) Expected signal enhancement in DP configuration for Al I at 265.3, 305.0, 308.2 nm and Al II at 281.6, 385.6, 466.3 nm lines for $E_1=E_2=78$ mJ, an interpulse delay of 4 μs and considering $N_{DP}=N_{SP}$ (see Eq. (1)). (b) Signal enhancement of the same lines experimentally measured. (c) Comparison of the measured (triangles) and predicted (squares) values, accounting for an increase (~7 times) of mass ablated in the DP configuration ($N_{DP}=7N_{SP}$).

function of the energy of the first laser pulse E_1. The volume of the crater in DP case is larger than that obtained in the SP by a factor 4–6, except in the case $E_1=13$ mJ where the volume in the two configurations is the same, within the experimental errors. Moreover, the growth of the volume with the pulse energy E_1 is different in the two cases, showing a steep increase in the DP case for low energies (represented in Fig. 8b).

In both the single- and double-pulse cases, a large amount of the material removed in the drilling is accumulated by melt flushing in a rim around the hole; during the drilling process, in fact, the vapor pressure at the bottom of the hole forces the molten material to climb the crater walls up to the target surface [26]. Since the density of molten and re-solidified material can be lower than the target, the volume of the material upper the target surface ($Volume_{up}$) may be higher than the volume drilled in the target ($Volume_{down}$). A similar result has been already found by Horn et al. [27] focusing a 266-nm Nd:YAG laser onto various metal surfaces and by Liu et al. [28] using a 266-nm Nd:YAG laser on a silicon target. In single-pulse craters, the ratio $Volume_{up}/Volume_{down}$ is in the range 1.8–2.5 while in the DP craters, except the case $E_1=13$ mJ where $Volume_{up}/Volume_{down}=1.8$ (very similar to the single-pulse craters), $Volume_{up}/Volume_{down}$ is in the range 0.8–1.1.

The change in density between the material above and under the surface does not allow the calculation of the effective ablated mass in the plume by the difference $Volume_{down}-Volume_{up}$.

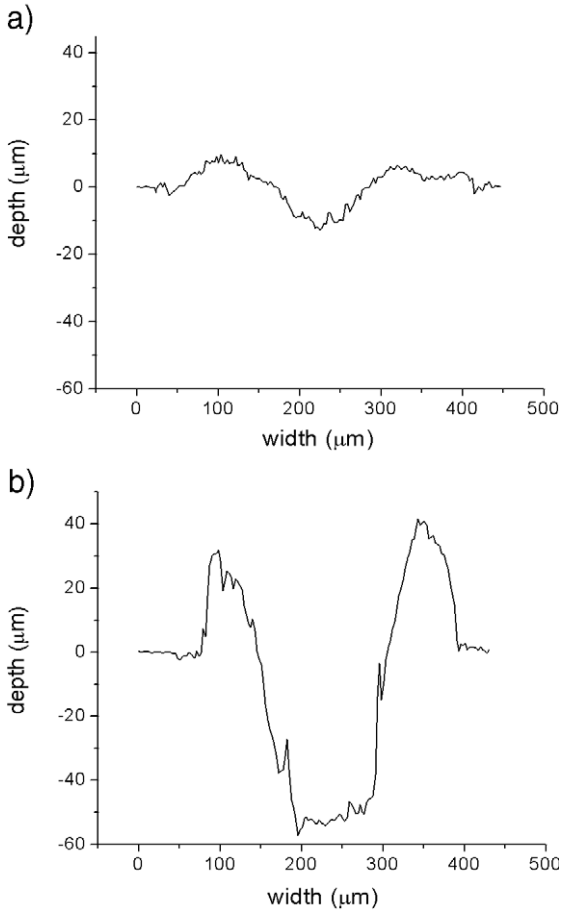

Fig. 7. Profile of the craters obtained in (a) single-pulse configuration (laser energy $E=E_1+E_2=156$ mJ) and (b) double-pulse configuration at the interpulse delay of 4 μs with laser energies $E_1=E_2=78$ mJ.

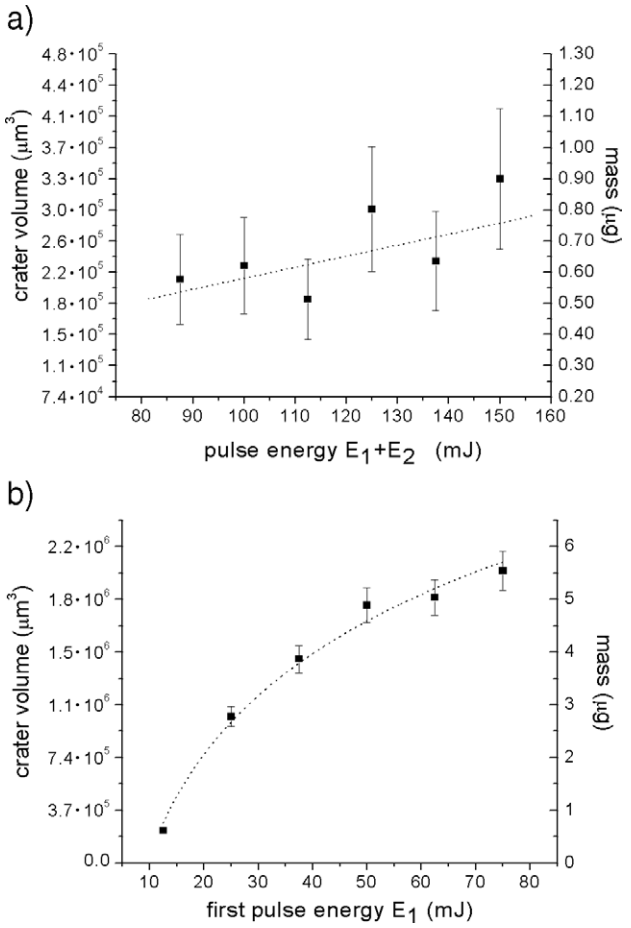

Fig. 8. Measured volume (μm^3) under the target surface and corresponding removed mass (μg) in (a) single-pulse configuration vs. the total pulse energy E_1+E_2 (the dotted line represents a linear fitting of the data) and in (b) double-pulse configuration vs. the energy E_1 of the first laser pulse (the dotted line represents a guide for the eye).

For this reason, we estimated the aluminum ablated mass M_{Al} (scaled by an arbitrary factor) from the measured LIBS intensity I_{ki} of the Al lines and from the calculated thermodynamical parameters of the plasma (T and n_e) using the formula:

$$M_{Al} = N_{Al} m_{Al} = \frac{F I_{ki} Z(T) \exp(E_k/k_B T)}{n(T, n_e) A_{ki} g_k} m_{Al} \quad (2)$$

where as in Eq. (1), N_{Al} is the total number of aluminum atoms, n is the fraction of the atoms corresponding to the considered emitting species (atomic or ionic), which can be calculated by the Saha equation using the experimental values of T and n_e; $Z(T)$ is the partition function of the species; E_k, g_k and A_{ki} are the upper level energy of the transition, its degeneracy and the corresponding transition probability; F is a factor dependent on the geometry and the spectral efficiency of the experimental setup and m_{Al} is the atomic mass of aluminum. Using Eq. (2), the ablated mass has been estimated (in arbitrary units) considering the LIBS intensities of Al I at 305.0 nm line and Al II at 281.6 nm line. The relative errors, calculated by the error propagation, between the values calculated from a single line, are of the order of ~20%.

The results obtained for superimposed pulses and for pulses delayed by 1 μs and 4 μs are shown in Fig. 9a, b and c, respectively. The results obtained for the other interpulse delays, not shown here, are qualitatively similar to Fig. 9b and c. These results confirm the qualitative trends already deduced from measurements of the crater volume.

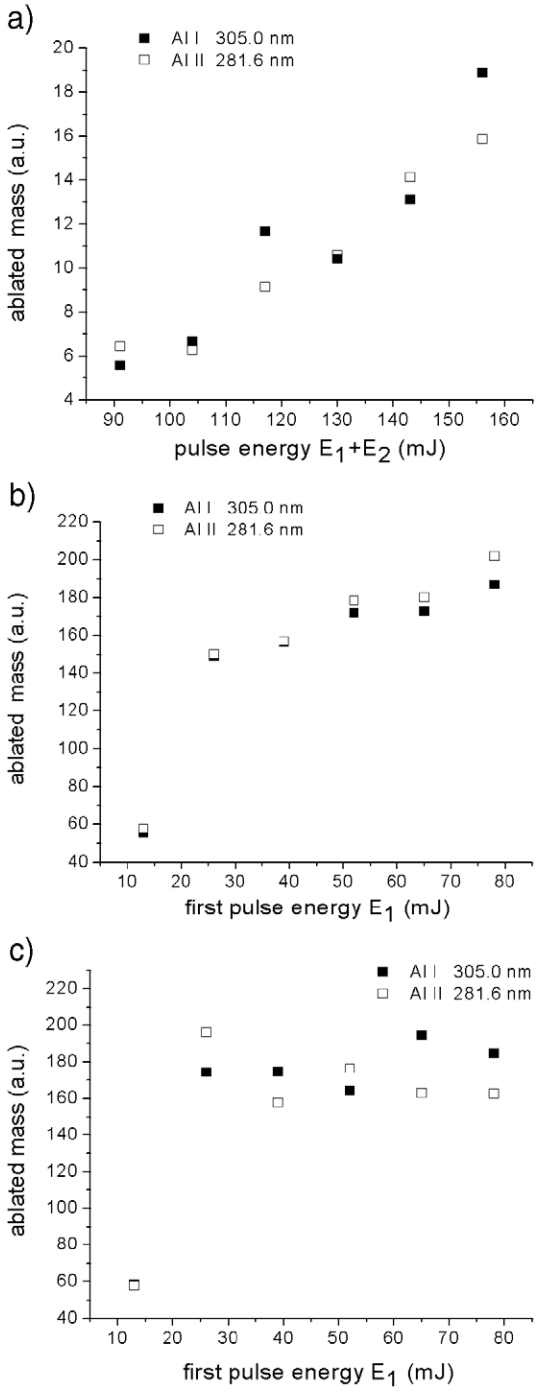

Fig. 9. Ablated mass, in arbitrary units, estimated by measured intensities of Al I at 305.0 nm and Al II at 281.6 nm lines in (a) single-pulse configuration vs. the total pulse energy E_1+E_2 and in (b) and (c) double-pulse configuration vs. the energy E_1 of the first laser pulse with an interpulse delay of 1 μs and 4 μs, respectively.

4. Discussion

The linear trends of crater volume and ablated mass with pulse energy shown in Figs. 8a and 9a (SP case) agree with previous works [27,29,30]. Both Horn et al. [27], focusing a Nd:YAG laser operating in its fourth harmonic (266 nm) on several metal targets (fluence in the range 3.5–35 J cm^{-2} depending on the sample), and Ducreux-Zappa and Mermet [29], analyzing a glass target with a Nd:YAG laser operating again at 266 nm (fluence in the range 5–37.5 J cm^{-2}) and with an XeCl laser operating at 308 nm (fluence in the range 27–75 J cm^{-2}), found a similar linear relation between the ablated mass from the target and the laser energy used. Similarly, Semerok et al. [30] focusing a Nd:YAG laser emitting at 532 nm on a copper target found an almost linear relation between crater volume and pulse energy ($V \propto E^{0.9}$), working at laser fluences more similar to our conditions (range 10–4500 J cm^{-2}).

On the other hand, the abrupt rise of crater volume and ablated mass with the first pulse energy in DP configuration (Figs. 8b and 9b–c) was not observed before and deserves a specific discussion. Clearly, such behavior is intimately connected with the physical mechanism originating the signal improvement in double-pulse experiments. Two mechanisms [8] can be considered to explain such increase, i.e. the pre-heating of the target and the reduction of the ambient gas density left by the first laser pulse.

Both these phenomena can produce a higher mass ablation, and then a higher signal, when the second laser pulse hits the target. The results here reported cannot exclude any of the two mechanisms; however, they can nevertheless give some interesting indication on the main physical processes occurring and on the optimal experimental setup to be used in the DP configuration.

In the pre-heating scenario, the higher mass removal in the DP configuration is due to the residual temperature of the target surface at the arrival time of the second laser pulse, which improves the ablation process. In fact, it has been observed that increasing the temperature of the target results in a signal enhancement [31].

It has been demonstrated [32] that the temperature of the target surface at the end of a laser pulse is approximately proportional to the total laser fluence on the target (the initial ambient temperature of the target is negligible). With increasing the laser intensity, the fluence reaching the target saturates, due to the plasma shielding. In principle, this effect could explain the roll-off of the ablated mass with the first pulse energy shown in Figs. 8b and 9b–c. However, both the ablation modeling of a Cu target in vacuum of Bogaerts et al. [33] and the investigations of Shannon et al. [34] on the laser ablation of several targets in argon atmosphere showed that such roll-off effect occurs at laser irradiances in the range of $2–3 \cdot 10^8$ W cm^{-2}. Similarly, Hrovatin and Mozina [35], focusing a Nd:YAG laser on a Al-epoxy films, found a roll-off threshold of $\sim 1.3 \cdot 10^8$ W cm^{-2}. Moreover, Shannon et al. [34] did not found significant differences of the roll-off threshold for the different matrix targets used. On the other hand, the roll-off observed in our configuration occurs at laser fluences at least one order of magnitude higher ($\sim 6 \cdot 10^9$ W cm^{-2}) than the above-mentioned laser-shielding thresholds; therefore, the increase of the target temperature does not seem to be able to explain our experimental results.

Moreover, the surface temperature would decrease very rapidly during the first hundreds of nanoseconds, reaching again the room temperature after about 1 μs [36]. Thus, the pre-heating mechanism, in theory, could play a role in the early 300–400 ns; however, in this range of interpulse delays the experimental findings show a LIBS signal enhancement much lower than the maximum, located at an interpulse delay of some microseconds [15], as shown in Fig. 3. This suggests that the persistency of a shielding of the first plasma up to an interpulse delay of 400 ns [37] hinders the pre-heating mechanism in the only interpulse range (0–400 ns) where it could be really important. These considerations seem to exclude the pre-heating from being the leading reason of the mass removal increase.

On the contrary, the hydrodynamical mechanism which produces the environment gas rarefaction in front of the target is effective on typical time scales much longer than the microsecond and is thus able to explain the signal enhancement observed even at an interpulse delay of 50 μs. Moreover, the hydrodynamical mechanism could also explain the roll-off of ablated mass vs. the laser pulse energy E_1. In a previous paper [14], we showed that the optimal buffer gas pressure for a single-pulse LIBS experiment on a Cu–Zn target is around 100 Torr, with the plasma emission decreasing for higher and lower pressures; such feature, together with the results of DP experiments performed at different buffer gas pressures, suggests that the signal enhancement in DP configuration is related to an improved laser ablation by the second laser pulse, due to the rarefied gas density inside the region encompassed by the shock wave produced by the first laser pulse. In DP LIBS, the ablated mass is greater (and the emission is higher) when the gas density inside the bubble approaches the optimum value. An estimation of the gas density in front of

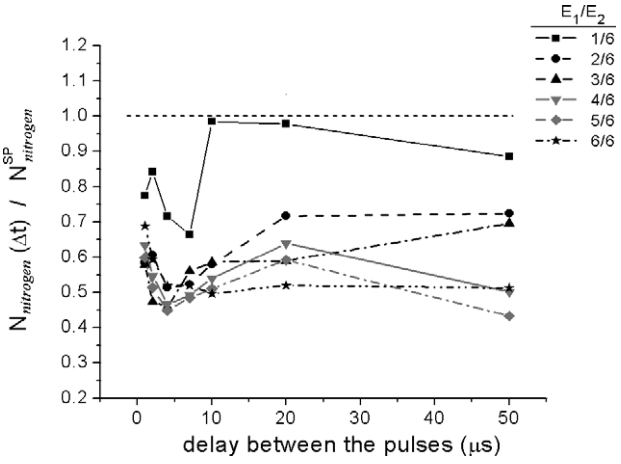

Fig. 10. Ratio of estimated nitrogen number density in DP configuration over the same value obtained in single-pulse configuration with a pulse energy $E = 78$ mJ, as a function of interpulse delays and for different E_1 energies. The data have been calculated from the N I at 744.3 nm line.

the target surface after the first laser pulse was given in Ref. [38], referring to the experimental conditions described in Ref. [13]; the value found was ~7% of the atmospheric gas density, in accordance with the model proposed.

Bearing this in mind, it is possible that in the conditions of the present experiment the pulse energy $E_1=13$ mJ is too low to bring the gas density close to the optimal value, while higher E_1 are obviously more effective. We can attain a qualitative validation of such an interpretation by comparing the number density of nitrogen atoms in the plume obtained in DP configuration at different interpulse delays (at pulse energies $E_1=13$, 26, 39, 52, 65, and 78 mJ and $E_2=78$ mJ) with the same value obtained in single-pulse configuration with an energy pulse $E_2=78$ mJ (see Fig. 10). The atom density has been estimated as in Eq. (2), resting on the approximation of spatially homogeneous plasma. Since the nitrogen is coming from the ambient gas and its abundance is not enriched by the second pulse, the ratio reported in Fig. 10 is a qualitative indication of the environment gas rarefaction in the bubble created by the first pulse. The experimental errors on the data (neglecting the systematical errors due to A_{ki} uncertainties) are of the order of 30% for $E_1=13$ mJ and of the order of 20% for the other energies.

The results suggest that the rarefaction behind the shock wave produced by a laser pulse of energy $E_1=13$ mJ is markedly lower ($0.7<y<1.0$) than the one obtained at higher laser energies ($0.4<y<0.7$), thus confirming our interpretation of the DP enhancement effect in terms of the reduction of the density of the ambient gas produced by the first laser pulse.

From the point of view of the optimization of the experimental setup in the DP configuration, an important corollary of these results is that the first pulse can be also conspicuously less energetic that the second one, without a substantial reduction of the LIBS signal enhancement. This consideration is particularly important in those cases where both the pulses are created by the same laser by successive Q-switches triggering [4,39,40]. In that case, it is preferable to adjust the delay between the two Q-switches triggering so that, the second pulse, which is more important in the removal of material from the target, is markedly higher than the first one. This result is in accordance with the work of Pichahchy et al. [39] who found that the best ratio of the pulses energy ratio E_2/E_1 is approximately 3 in the case of LIBS analysis of metals under water.

5. Conclusions

The influence of the energy of the first laser pulse in the DP collinear LIBS configuration was studied at different interpulse delays varying between 0 and 50 μs; a substantial improvement of the LIBS signal, with respect to the single-pulse configuration, was obtained for $E_1=1/3E_2$, while the signal steeply decreased for lower values of the E_1/E_2 ratio (fluence of the first laser lower than $\sim 6\cdot 10^9$ W cm^{-2}).

The measured small increase of the temperature in DP configuration can explain the trend of the signal with the upper level energy of the transition but is unable to justify the high enhancements observed.

On the other hand, these enhancements can be correlated to an increase of the mass removed in DP configuration, as suggested by the deeper craters measured and the estimated ablated mass (scaled by an arbitrary factor).

The results reported in this paper seem consistent with the interpretation of the signal enhancement in double-pulse configuration in terms of the reduction of the density of the ambient left by the first laser pulse. These findings, besides giving a further insight on the processes underlying laser interaction with matter in double-pulse configuration, can also be useful for optimization of actual LIBS experiments in a number of practical applications.

References

[1] S. Nakamura, Y. Ito, K. Sone, H. Hiraga, K. Kaneko, Determination of an iron suspension in water by laser-induced breakdown spectroscopy with two sequential laser pulses, Anal. Chem. 68 (1996) 2981–2986.
[2] L. St-Onge, M. Sabsabi, P. Cielo, Analysis of solids using laser induced plasma spectroscopy in double-pulse mode, Spectrochim. Acta Part B 53 (1998) 407–415.
[3] L. St-Onge, V. Detalle, M. Sabsabi, Enhanced laser-induced breakdown spectroscopy using the combination of fourth-harmonic and fundamental Nd:YAG laser pulses, Spectrochim. Acta Part B 57 (2002) 121–135.
[4] R. Noll, R. Sattmann, V. Sturm, S. Winkelmann, Space- and time-resolved dynamics of plasmas generated by laser double pulses interacting with metallic samples, J. Anal. At. Spectrom. 19 (2004) 419–428.
[5] F. Colao, V. Lazic, R. Fantoni, S. Pershin, A comparison of single and double pulse laser-induced breakdown spectroscopy of aluminum samples, Spectrochim. Acta Part B 57 (2002) 1167–1179.
[6] S.M. Angel, D.N. Stratis, K.L. Eland, T. Lai, M.A. Berg, D.M. Gold, LIBS using dual- and ultra-laser pulses, Fresenius' J. Anal. Chem. 369 (2001) 320–327.
[7] D.N. Stratis, K.L. Eland, S.M. Angel, Dual-pulse LIBS using a preablation spark for enhanced ablation and emission, Appl. Spectrosc. 54 (2000) 1270–1274.
[8] D.N. Stratis, K.L. Eland, S.M. Angel, Effect of pulse delay time on a pre-ablation dual-pulse LIBS plasma, Appl. Spectrosc. 55 (2001) 1297–1303.
[9] D.N. Stratis, K.L. Eland, S.M. Angel, Enhancement of aluminum, titanium, and iron in glass using pre-ablation spark dual-pulse LIBS, Appl. Spectrosc. 54 (2000) 1719–1726.
[10] J. Scaffidi, J. Pender, B. Pearman, S.R. Goode, B.W. Colston Jr., J.C. Carter, S.M. Angel, Dual-pulse LIBS combinations of femtosecond and nanosecond laser pulses, Appl. Opt. 42 (2003) 6099–6106.
[11] C. Gautier, P. Fichet, D. Menut, J.L. Lacour, D. L'Hermite, J. Dubessy, Study of the double-pulse setup with an orthogonal beam geometry for laser-induced breakdown spectroscopy, Spectrochim. Acta Part B 59 (2004) 975–986.
[12] C. Gautier, P. Fichet, D. Menut, J.L. Lacour, D. L'Hermite, J. Dubessy, Quantification of the intensity enhancements for the double-pulse laser induced breakdown spectroscopy in the orthogonal beam geometry, Spectrochim. Acta Part B 60 (2005) 265–276.
[13] M. Corsi, G. Cristoforetti, M. Giuffrida, M. Hidalgo, S. Legnaioli, V. Palleschi, A. Salvetti, E. Tognoni, C. Vallebona, 3D-analysis of laser induced plasmas in single and double pulse configuration, Spectrochim. Acta Part B 59 (2004) 723–735.
[14] G. Cristoforetti, S. Legnaioli, V. Palleschi, A. Salvetti, E. Tognoni, Influence of ambient gas pressure on laser-induced breakdown spectroscopy technique in the parallel double-pulse configuration, Spectrochim. Acta Part B 59 (2004) 1907–1917.
[15] G. Cristoforetti, S. Legnaioli, V. Palleschi, A. Salvetti, E. Tognoni, Characterization of a collinear double pulse laser-induced plasma at

several ambient gas pressures by spectrally- and time-resolved imaging, Appl. Phys. B (2005) 559–568.
[16] V.N. Ray, F.Y. Yueh, J.P. Singh, Study of laser induced breakdown emission from liquid under double pulse excitation, Appl. Opt. 42 (2003) 2094–2101.
[17] A. Ciucci, V. Palleschi, S. Rastelli, A. Salvetti, D.P. Singh, E. Tognoni, Effect of imperfect focusing in laser-induced plasma spectroscopy measurements, Il Nuovo Cimento D 20 (1998) 1469–1478.
[18] J.A. Aguilera, J. Bengoechea, C. Aragon, Spatial characterization of laser induced plasmas obtained in air and argon with different laser focusing distances, Spectrochim. Acta Part B 59 (2004) 461–469.
[19] P.A. Benedetti, V. Evangelista, D. Guidarini, S. Vestri, Electronic multiconfocal-points microscopy, SPIE Proc. 2412 (1995) 56–62.
[20] P.A. Benedetti, W. Evangelista, D. Guidarini, S. Vestri, Method for the acquisition of images by confocal microscopy, U.S. Patent 6.016.367, 2000.
[21] J. Ashkenazy, R. Kipper, M. Caner, Spectroscopic measurements of electron density of capillary plasma based on Stark broadening of hydrogen lines, Phys. Rev. A 43 (1991) 5568–5574.
[22] H.R. Griem, Spectral Line Broadening by Plasma, Academic, New York, 1974.
[23] K.M. Lo, N.H. Cheung, ArF laser-induced plasma spectroscopy for part-per-billion analysis of metal ions in aqueous solutions, Appl. Spectrosc. 56 (6) (2002) 682–688.
[24] O. Samek, D.C.S. Beddows, J. Kaiser, S.V. Kukhlevsky, M. Lika, H.H. Telle, J. Young, Application of laser-induced breakdown spectroscopy to in situ analysis of liquid samples, Opt. Eng. 39 (8) (2000) 2248–2262.
[25] S. Yalcin, D.R. Crosley, G.P. Smith, G.W. Faris, Influence of ambient conditions on the laser air spark, Appl. Phys. B 68 (1999) 121–130.
[26] C. Korner, R.M. Mayerhofer, M. Hartman, H.W. Bergmann, Physical and material aspects in using visible laser pulses of nanosecond duration for ablation, Appl. Phys. A 63 (1996) 123–131.
[27] I. Horn, M. Guillong, D. Gunther, Wavelength dependant ablation rates for metals and silicate glasses using homogenized laser beam profiles—implications for LA-IPC-MS, Appl. Surf. Sci. 182 (2001) 91–102.
[28] H.C. Liu, X.L. Mao, J.H. Yoo, R.E. Russo, Early phase laser induced plasma diagnostics and mass removal during single-pulse laser ablation of silicon, Spectrochim. Acta Part B 54 (1999) 1607–1624.
[29] M. Ducreux-Zappa, J.M. Mermet, Analysis of glass by UV laser ablation inductively coupled plasma atomic emission spectrometry: Part I. Effects of the laser parameters on the amount of ablated material and the temporal behavior of the signal for different types of laser, Spectrochim. Acta Part B 51 (1996) 321–332.
[30] A. Semerok, B. Sallè, J.F. Wagner, G. Petite, Femtosecond, picosecond, and nanosecond laser microablation: laser plasma and crater investigation, Laser Part. Beams 20 (2002) 67–72.
[31] S. Palanco, L.M. Cabalin, D. Romero, J.J. Laserna, Infrared laser ablation and atomic emission spectrometry of stainless steel at high temperatures, J. Anal. At. Spectrom. 14 (1999) 1883–1887.
[32] J.C. Miller, R.F. Haglund, Laser Ablation and Desorption, Academic Press, London, 1988, p. 178.
[33] A. Bogaerts, Z. Chen, R. Gijbels, A. Vertes, Laser ablation for analytical sampling: what can we learn from modeling? Spectrochim. Acta Part B 58 (2003) 1867–1893.
[34] M.A. Shannon, X.L. Mao, A. Fernandez, W.T. Chan, R. Russo, Laser ablation mass removal versus incident power density during solid sampling for inductively coupled plasma atomic emission spectroscopy, Anal. Chem. 67 (1995) 4522–4529.
[35] R. Hrovatin, J. Mozina, Optodynamic aspect of a pulsed laser ablation process, Appl. Surf. Sci. 86 (1995) 213–218.
[36] J.R. Ho, C.P. Grigoropoulos, J.A.C. Humphrey, Computational study of heat transfer and gas dynamics in the pulsed laser evaporation of metals, J. Appl. Phys. 78 (1995) 4696–4708.
[37] H.W. Bergmann, Excimer laser induced surface modifications and matter interaction using double-pulse-technique (DPT), Appl. Surf. Sci. 96–98 (1996) 287–295.
[38] M. Corsi, G. Cristoforetti, M. Giuffrida, M. Hidalgo, S. Legnaioli, V. Palleschi, A. Salvetti, E. Tognoni, C. Vallebona, Authors' reply to Wen et al. comment, Spectrochim. Acta Part B 60 (2005) 872–875.
[39] A.E. Pichahchy, D.A. Cremers, M.J. Ferris, Elemental analysis of metals under water using laser-induced breakdown spectroscopy, Spectrochim. Acta Part B 52 (1997) 25–39.
[40] R. Sattmann, V. Sturm, R. Noll, Laser-induced breakdown spectroscopy of steel samples using multiple Q-switch Nd:YAG laser pulses, J. Phys. D: Appl. Phys. 28 (1995) 2181–2187.